

Non-Standard Interactions of Supernova Neutrinos and Mass Ordering Ambiguity at DUNE

Sudip Jana^{1,*} and Yago Porto^{2,†}

¹Max-Planck-Institut für Kernphysik, Saupfercheckweg 1, 69117 Heidelberg, Germany

²Centro de Ciências Naturais e Humanas, Universidade Federal do ABC, 09210-170, Santo André, SP, Brazil

We show that non-standard neutrino interactions (NSI) can notably modify the pattern of resonant flavor conversion of neutrinos within supernovae and significantly impact the neutronization burst signal in forthcoming experiments such as the Deep Underground Neutrino Experiment (DUNE). The presence of NSI can invert the energy levels of neutrino matter eigenstates and even induce a new resonance in the inner parts close to the proto-neutron star. We demonstrate how DUNE can use these new configurations of energy levels to have sensitivity to NSIs down to $\mathcal{O}(0.1)$. We also elucidate how the effect may result in a puzzling confusion of normal and inverted mass orderings by highlighting the emergence or vanishing of the neutronization peak, which distinguishes between the two mass orderings. Potential implications are analyzed thoroughly.

Introduction.— In recent decades, extensive efforts and data from solar, atmospheric, reactor, and accelerator neutrino experiments have provided robust evidence for neutrino oscillations, indicating the presence of neutrino masses and mixing. However, the origin of these phenomena remains unestablished, leaving room for potential new physics, particularly in the form of non-standard neutrino interactions (NSIs). First introduced by Wolfenstein in 1978 [1], NSIs have been the subject of intense scrutiny since then, providing an avenue for exploring new aspects of neutrino physics. These interactions involve higher-dimensional operators with neutrinos and matter, as represented by the equations:

$$\begin{aligned}\mathcal{L}_{\text{NC}} &= -2\sqrt{2}G_F \sum_{f,P,\alpha,\beta} \varepsilon_{\alpha\beta}^{f,P} (\bar{\nu}_\alpha \gamma^\mu P_L \nu_\beta) (\bar{f} \gamma_\mu P f) \\ \mathcal{L}_{\text{CC}} &= -2\sqrt{2}G_F \sum_{f,P,\alpha,\beta} \varepsilon_{\alpha\beta}^{f,P} (\bar{\nu}_\alpha \gamma^\mu P_L \ell_\beta) (\bar{f} \gamma_\mu P f')\end{aligned}\quad (1)$$

where ε represents the strength of NSI relative to the weak scale, $P \in P_L, P_R$ indicates chirality projection operators and the sum is over matter fermions $f, f' \in e, u, d$. Such NSIs modify the matter potential experienced by neutrinos, adding substantial intricacy to the determination of neutrino oscillation parameters. For instance, the existence of NSI introduces ambiguity in the determination of θ_{12} from the solar neutrino data [2]. Furthermore, NSI effects have been shown to alleviate the tension between solar and KamLAND data, as it flattens the solar neutrino spectrum at high energies (> 3 MeV) and generates larger day-night asymmetry [3]. In this study, we advocate for the utilization of supernova neutrinos to investigate the influence of these NSI on the precise determination of neutrino oscillation parameters.

During a supernova (SN) explosion, as the progenitor's core collapses to form a neutron star, about 10^{53} erg of gravitational binding energy is released in the form of

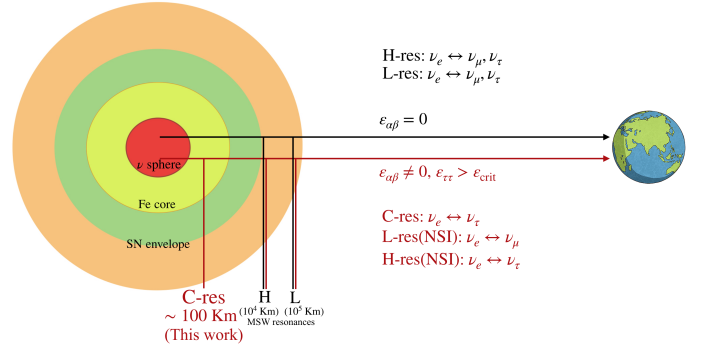


FIG. 1. A simplified picture of flavor conversions of supernova neutrinos in presence of NSI.

neutrinos [4–8]. Originating in the SN core with energies in the tens of MeV, these neutrinos travel through the stellar mantle and envelope, undergoing modifications in mixing and oscillations through neutrino-matter interactions¹ [1, 10–12]. The consequences of neutrino propagation in the SN-dense environment offer significant potential for probing new physics, and these effects are observable by flavor-sensitive Earth-based detectors [13–22]. A galactic SN, a rare event in the Milky Way occurring once or twice per century, was last observed in 1987 from the Large Magellanic Cloud, 51 Kpc away [23–26]. Neutrino detectors recorded about 25 $\bar{\nu}_e$ events during that event, significantly advancing our understanding of core-collapse processes and neutrino emission [27–30]. Future detectors, especially the Deep Underground Neutrino Experiment (DUNE), are anticipated to capture hundreds of thousands of events in various channels during a galactic supernova [31–36], with DUNE's unique capability to detect a clean ν_e signal in the critical first 40 ms after core bounce, known as the neutronization burst phase [36–38]. In this article, we investigate the features of

* E-mail:sudip.jana@mpi-hd.mpg.de

† E-mail:yago.porto@ufabc.edu.br

¹ Matter effects can also influence the evolution of high-energy astrophysical neutrinos with energies greater than 100 TeV [9].

neutrino emission in the neutronization burst phase, elucidate the anticipated resonant flavor conversion within the stellar envelope triggered by NSI [cf. Fig. 1] and discuss the crucial role of DUNE in exploring new physics impacting supernova neutrinos.

Dynamics of Resonant Flavor Conversions.–

Understanding the flavor composition of SN neutrinos reaching the Earth during the neutronization burst phase requires monitoring how the initial fluxes generated in the core evolve while traveling outward within the star (see Appendix for details). In the dense environment where neutrinos propagate inside the star, vacuum oscillations are suppressed. However, the density variation in the way out of the SN instigates a flavor evolution dictated by a time (or space) dependent Hamiltonian that can trigger Mikheyev-Smirnov-Wolfenstein (MSW) resonant flavor conversion in specific layers of the matter profile [1, 10–12, 39].

Assuming that neutrinos propagate radially outwards, the evolution equation for the flavor state $\nu = (\nu_e, \nu_\mu, \nu_\tau)^T$ is

$$i \frac{d}{dr} \nu = \mathcal{H} \nu. \quad (2)$$

\mathcal{H} is the Hamiltonian in the flavor basis given by

$$\mathcal{H} = \frac{1}{2E} U \begin{pmatrix} 0 & 0 & 0 \\ 0 & \Delta m_{21}^2 & 0 \\ 0 & 0 & \Delta m_{31}^2 \end{pmatrix} U^\dagger + V_e \begin{pmatrix} 1 & 0 & 0 \\ 0 & 0 & 0 \\ 0 & 0 & 0 \end{pmatrix}, \quad (3)$$

where E and U denote the neutrino energy and the Pontecorvo-Maki-Nakagawa-Sakata (PMNS) matrix. The matter potential due to charged current interactions can be expressed as

$$V_e = \sqrt{2} G_F \frac{\rho}{m_N} Y_e, \quad (4)$$

where Y_e is the electron number fraction and ρ is the matter density (see Fig. 7 in the Appendix for the profile of ρ and Y_e). The antineutrino Hamiltonian is similar to \mathcal{H} , with the only difference being that the matter potential inverts sign $\bar{V}_e = -V_e$.

In dense matter, $\rho > 10^5$ g/cm³, V_e is much bigger than all other matrix elements in Eq. 3, suppressing mixing and making ν_e the heaviest effective eigenstate in matter, $\nu_e \approx \nu_3^m$ for normal ordering (NO) and $\nu_e \approx \nu_2^m$ for inverted ordering (IO), the superscript m denotes an effective eigenstate in matter. In a vacuum, however, ν_e is mostly associated with ν_1 . Therefore, as matter density decreases, so does V_e , and ν_e will transit from ν_3^m (ν_2^m) to ν_1^m . In doing so, it has to cross energy levels twice for NO ($\nu_3^m \rightarrow \nu_2^m \rightarrow \nu_1^m$) and once for IO ($\nu_2^m \rightarrow \nu_1^m$). The level crossing diagram is shown in Fig. 2. The red dashed line follows the evolution of the electron flavor, ν_e on the right of $V_e = 0$ and $\bar{\nu}_e$ on the left. Note that $\bar{\nu}_e \approx \bar{\nu}_1^m$ in the inner regions, and there is no level crossing for antineutrinos in NO, while there is one level crossing in IO:

$\bar{\nu}_3^m \rightarrow \bar{\nu}_1^m$. While ν_e and $\bar{\nu}_e$ are effective eigenstates in the SN environment, ν_μ , ν_τ , and their antiparticles are not effective eigenstates due to near maximal vacuum mixing. In this situation, it is convenient to diagonalize the $\nu_\mu - \nu_\tau$ subspace and work with the effective eigenstates ν'_μ , ν'_τ , and their antiparticles. The primed states have constant energy levels as a function of V_e , as shown in Fig. 2.

The crossing $\nu_e \leftrightarrow \nu'_\tau$ is called H -resonance and occurs when

$$V_e(\rho_H) \approx \frac{\Delta m_{31}^2}{2E} \cos \theta_{13}, \quad (5)$$

which corresponds to higher densities compared to the L -resonance, $\nu_e \leftrightarrow \nu'_\mu$, that happens when

$$V_e(\rho_L) \approx \frac{\Delta m_{21}^2}{2E} \cos \theta_{12}. \quad (6)$$

Note that Eq. 5 is satisfied for neutrinos in NO and for antineutrinos in IO ($\Delta m_{31}^2 = -|\Delta m_{31}^2|$ and V_e is negative) while Eq. 6 is satisfied only for neutrinos in both orderings. Using the profile in Fig. 7, and oscillation parameters from [40], the H -resonance happens at $r \sim 10^4$ Km (ρ_H in the range $10^3 - 10^4$ g/cm³) and the L -resonance at $r \sim 10^5$ Km ($\rho_L \sim 1 - 10$ g/cm³). Efficient resonant conversion only happens if neutrinos cross resonance layers adiabatically [41]. We will assume perfect adiabaticity of the H - and L -resonances so that transitions between distinct energy eigenstates are negligible. Moreover, the produced flux during the neutronization burst phase is mostly $\nu_e \approx \nu_3^m$ (ν_2^m) for NO (IO). Due to adiabaticity, the initial eigenstates are preserved and reach vacuum as ν_3 (ν_2). Consequently, for NO only $|U_{e3}|^2 \approx 0.02$ of the initial ν_e flux, F_e^i , survives and reaches Earth, and some amount of ν_e , $(1 - |U_{e3}|^2) F_x^i \approx 0.98 F_x^i$, comes from the conversion of non-electron flavors, $F_\mu^i = F_\tau^i = F_x^i$:

$$F_e^{NO} = |U_{e3}|^2 F_e^i + (1 - |U_{e3}|^2) F_x^i \approx 0.02 F_e^i + 0.98 F_x^i. \quad (7)$$

Similarly for IO,

$$F_e^{IO} = |U_{e2}|^2 F_e^i + (1 - |U_{e2}|^2) F_x^i \approx 0.3 F_e^i + 0.7 F_x^i. \quad (8)$$

Due to F_e^i being approximately ten times F_x^i at the neutronization peak, the ν_e flux is greater in the Inverted Ordering (IO) than in the Normal Ordering (NO) during the initial 20 milliseconds of neutrino emission. This disparity enhances the visibility of the peak in neutrino detectors for the IO scenario. In the following sections, we will analyze signals derived from flux equations (7) and (8) in DUNE and discuss the presence or absence of the peak as a discriminative criterion between the two mass orderings.

Effect of NSI on the Energy Levels.– The introduction of NSIs has a pronounced impact on the configuration of energy levels and the flavor composition of

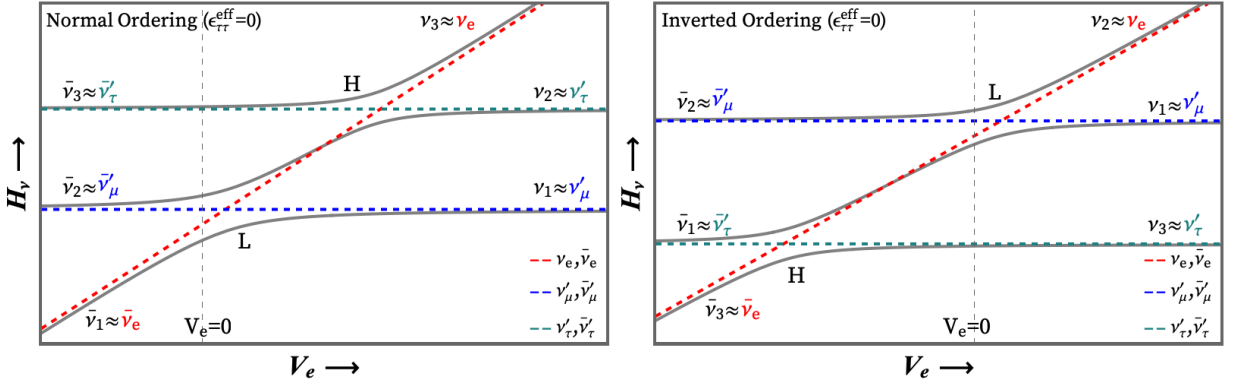


FIG. 2. Configuration of energy levels for neutrinos and antineutrinos for NO (left) and IO (right). For each panel, neutrino lines are shown for positive V_e , while antineutrinos are plotted with negative V_e . The location of the MSW resonances is indicated by the letters L and H . Solid lines represent the effective matter eigenstates, while the dashed lines follow the track of flavor states. Matter eigenstates mix with different flavors at different locations; this is shown by the flavor tags in red, blue, and green colors.

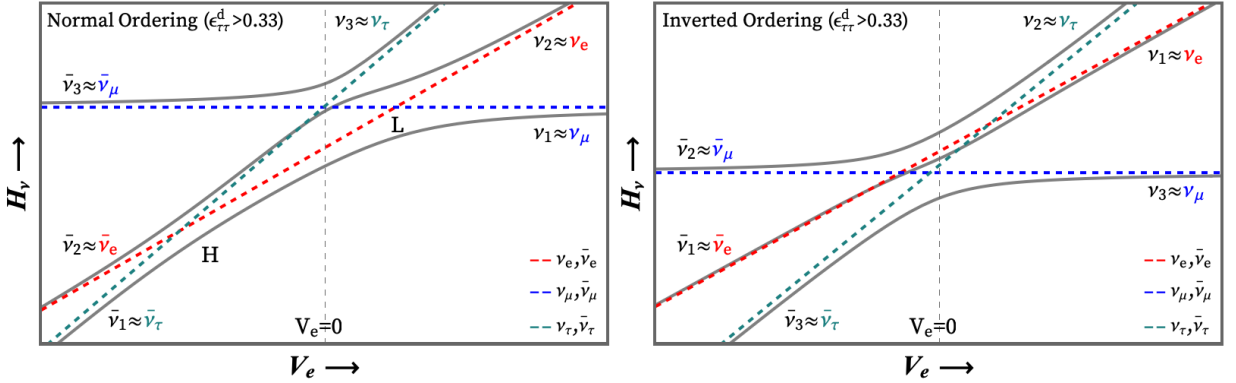


FIG. 3. Configuration of energy levels for neutrinos and antineutrinos for NO (left) and IO (right) with the inclusion of $\epsilon_{\tau\tau}^d > 0.33$. See text for details.

SN neutrinos detected on Earth. To demonstrate this effect, an additional energy term involving NSI parameters must be incorporated into the Hamiltonian mentioned in Eq. 3. Our focus here is on NSI specifically influencing ν_τ , potentially originating from interactions with electrons, u -quarks, and d -quarks. Recent systematic investigations indicate the feasibility of obtaining substantial values for $\epsilon_{\tau\tau}$ in various radiative neutrino mass models [42]. It is important to note that the approach to ν_μ NSI is analogous and yields numerically equivalent results.

The effective strength of the NSI parameter $\epsilon_{\tau\tau}^{\text{eff}}$ can be expressed in relation to interactions involving electrons, u -quarks, and d -quarks as follows:

$$\epsilon_{\tau\tau}^{\text{eff}} = \epsilon_{\tau\tau}^e + (2\epsilon_{\tau\tau}^u + \epsilon_{\tau\tau}^d) \frac{n_p}{n_e} + (\epsilon_{\tau\tau}^u + 2\epsilon_{\tau\tau}^d) \frac{n_n}{n_e}. \quad (9)$$

In various models of neutrino mass, new interactions emerge, giving rise to diverse NSI scenarios where $\epsilon_{\tau\tau}^u$, $\epsilon_{\tau\tau}^e$, or $\epsilon_{\tau\tau}^d$ may be exclusively generated, or in certain instances, combinations of two NSIs or all three NSIs. For instance, a scalar leptoquark with Standard Model gauge quantum numbers $(3, 2, 1/6)$, denoted as \tilde{R}_2 , can

induce only $\epsilon_{\tau\tau}^d$, while the leptoquark R_2 with charges $(3, 2, 7/6)$ exclusively leads to $\epsilon_{\tau\tau}^u$. On the other hand, the leptoquark S_3 with charges $(\bar{3}, 3, 1/3)$ can give rise to both $\epsilon_{\tau\tau}^d$ and $\epsilon_{\tau\tau}^u$. Further elaboration on these scenarios can be found in the detailed discussion provided in reference [42]. To optimize the signal, we exclusively consider quark NSIs here. Although leptonic NSIs may have some impact, they are expected to be less significant compared to quark NSIs, and therefore, they do not affect the phenomenology we are concentrating on. If only $\epsilon_{\tau\tau}^d$ exhibits a non-zero value, and under the condition of charge neutrality ($n_p = n_e$), we obtain:

$$\epsilon_{\tau\tau}^{\text{eff}} = \epsilon_{\tau\tau}^d \left(\frac{2 - Y_e}{Y_e} \right). \quad (10)$$

Considering non-zero values of $\epsilon_{\tau\tau}^u$, we obtain:

$$\epsilon_{\tau\tau}^{\text{eff}} = \epsilon_{\tau\tau}^u \left(\frac{1 + Y_e}{Y_e} \right). \quad (11)$$

Now, we focus on the region of the SN matter profile where H - and L - resonance occur, specifically for $r >$

10^4 Km. In this particular zone, $Y_e = 0.5$ (see Fig. 7 in the Appendix). The existence of either $\varepsilon_{\tau\tau}^d$ or $\varepsilon_{\tau\tau}^u > 0.33$ indicates that the effective matter potential for ν_τ surpasses that of ν_e , thereby modifying the dynamics of flavor conversion. The Hamiltonian in the presence of NSI is expressed as follows:

$$\mathcal{H}^{NSI} = \frac{1}{2E} U \begin{pmatrix} 0 & 0 & 0 \\ 0 & \Delta m_{21}^2 & 0 \\ 0 & 0 & \Delta m_{31}^2 \end{pmatrix} U^\dagger + V_e \begin{pmatrix} 1 & 0 & 0 \\ 0 & 0 & 0 \\ 0 & 0 & 3\varepsilon_{\tau\tau}^{u,d} \end{pmatrix}. \quad (12)$$

For $\varepsilon_{\tau\tau}^{u,d} > 0.33$, ν_τ is the heaviest eigenstate in matter, $\nu_\tau \approx \nu_3^m(\nu_2^m)$ for NO (IO). Hence, the main difference from the standard case is that ν_e starts as the second heaviest eigenstate, $\nu_e \approx \nu_2^m(\nu_1^m)$ for NO (IO), see Fig. 3. For NO, ν_e crosses level once through a L -resonance, $\nu_2^m \rightarrow \nu_1^m$, at densities given by Eq. 6. While for IO, ν_e is already produced as ν_1^m and reaches vacuum mostly as ν_1 without crossing levels. For antineutrinos, $\bar{\nu}_e \approx \bar{\nu}_2^m(\bar{\nu}_1^m)$, and crosses levels only for NO, via H -resonance. In this case, however, the potential of ν_τ , $V_\tau = \varepsilon_{\tau\tau} V_e$, is higher than V_e , so the difference $V_e - V_\tau$ is negative. The resonance condition is found by modifying Eq. 5 with $V_e \rightarrow (1 - \varepsilon_{\tau\tau})V_e$. Neutrinos fail to satisfy this new condition in NO. However, antineutrinos in NO can fulfill this condition since their potentials exhibit an inverted sign, denoted as $\bar{V}_e = -V_e$. Furthermore, the eigenstates are not represented in the primed basis, as the potential for ν_τ significantly surpasses the mixing terms, distinctly separating ν_μ and ν_τ .

Assuming perfect adiabaticity of H - and L - resonances, we find the final flux for both orderings:

$$F_e^{NO}(\varepsilon_{\tau\tau}^{u,d} > 0.33) = |U_{e2}|^2 F_e^i + (1 - |U_{e2}|^2) F_x^i \approx 0.3 F_e^i + 0.7 F_x^i, \quad (13)$$

and,

$$F_e^{IO}(\varepsilon_{\tau\tau}^{u,d} > 0.33) = |U_{e1}|^2 F_e^i + (1 - |U_{e1}|^2) F_x^i \approx 0.7 F_e^i + 0.3 F_x^i. \quad (14)$$

It is noteworthy that Eq.13 is equivalent to Eq.8 since, in both instances, ν_e is generated as ν_2^m . Consequently, the neutronization burst phase in the NO scenario with NSI and the standard IO scenario without NSI are indistinguishable. In the next sections, we analyze the signals from Eq. 13 and Eq. 14 at DUNE, emphasizing potential confusion in discerning between the two mass orderings in the presence of NSI.

New Resonances triggered by NSI.— We will now explore scenarios in which NSI can induce an additional resonance, designated as the C -resonance, alongside the existing L - and H - resonances. While examining NSI within the range $0.1 < \varepsilon_{\tau\tau}^{u,d} < 0.33$, we find that it influences the flavor evolution of neutrinos during the neutronization burst phase. Despite such values of $\varepsilon_{\tau\tau}^{u,d}$ not modifying the energy level pattern in the region $r > 10^3$ Km where L - and H -resonances occur ($Y_e \approx 0.5$), it does alter the energy levels inside the iron core ($r < 10^3$ Km) where neutrinos are produced ($0.2 < Y_e < 0.5$). In

this configuration, the C - resonance emerges inside the iron core, as illustrated in Fig. 4.

In order to examine the emergence of the C -resonance, we rewrite Eq. 12 by incorporating the expression for $\varepsilon_{\tau\tau}$ from Eq. 10 for d -quark NSI. Here, we concentrate exclusively on the matter potential term, which dominates over the vacuum term in regions of high core densities:

$$\mathcal{H}^{NSI} \approx V_e \begin{pmatrix} 1 & 0 & 0 \\ 0 & 0 & 0 \\ 0 & 0 & \varepsilon_{\tau\tau}^d \left(\frac{2-Y_e}{Y_e} \right) \end{pmatrix}. \quad (15)$$

Note that our focus here is on d -quark NSI. Nevertheless, the qualitative outcomes remain similar for u -quark NSI due to the resemblance between Eq. 10 and Eq. 11. In the subsequent section, we analyze the consequential effects by concurrently considering NSIs involving both d -quark and u -quark. Using the Y_e values from Fig. 7 (See Appendix for details), a level crossing occurs within the range of 50 to 1000 Km for $0.1 < \varepsilon_{\tau\tau}^d < 0.33$ as Y_e transitions from 0.2 to 0.5. Prior to the crossing point, $\varepsilon_{\tau\tau}^d (2 - Y_e)/Y_e > 1$, rendering ν_τ as the heaviest state, and ν_e as the second heaviest: $\nu_e \approx \nu_2^m(\nu_1^m)$ for NO (IO). Subsequent to the crossing point, the scenario inverts with $\varepsilon_{\tau\tau}^d (2 - Y_e)/Y_e < 1$, causing the energy levels of ν_e and ν_τ to intersect, as depicted in Fig. 4. This crossing can result in resonant conversion if we introduce off-diagonal NSI² $\varepsilon_{e\tau}$ and couple ν_e and ν_τ states:

$$\mathcal{H}^{NSI} \approx V_e \begin{pmatrix} 1 & 0 & \varepsilon_{e\tau}^d \left(\frac{2-Y_e}{Y_e} \right) \\ 0 & 0 & 0 \\ \varepsilon_{e\tau}^d \left(\frac{2-Y_e}{Y_e} \right) & 0 & \varepsilon_{\tau\tau}^d \left(\frac{2-Y_e}{Y_e} \right) \end{pmatrix}. \quad (16)$$

In such a scenario, the resonance condition can be expressed as

$$\varepsilon_{\tau\tau}^d \left(\frac{2 - Y_e}{Y_e} \right) = 1, \quad (17)$$

and can be satisfied by both neutrinos and antineutrinos simultaneously. Furthermore, Eq. 17 is independent of matter density, energy, and mass orderings. The adiabaticity condition is now formulated and can be expressed as

$$\gamma_C = \left| \frac{4(\mathcal{H}_{e\tau}^{NSI})^2}{\mathcal{H}_{\tau\tau}^{NSI} - \mathcal{H}_{ee}^{NSI}} \right| \approx \left| \frac{16V_e(\varepsilon_{e\tau}^d)^2}{Y_e \dot{Y}_e (1 + \varepsilon_{\tau\tau}^d)^3} \right| > 1. \quad (18)$$

Eq. 18 is satisfied for very small values of off-diagonal NSI: $\varepsilon_{e\tau} > 10^{-5}$. The resonance is partially adiabatic for $\varepsilon_{e\tau}$ values within the range of 10^{-6} to 10^{-5} . In the limit

² Significant flavor off-diagonal NSI can resolve discrepancies in the determination of the standard CP-phase δ_{CP} between the NO ν A and T2K long-baseline accelerator experiments [43, 44].

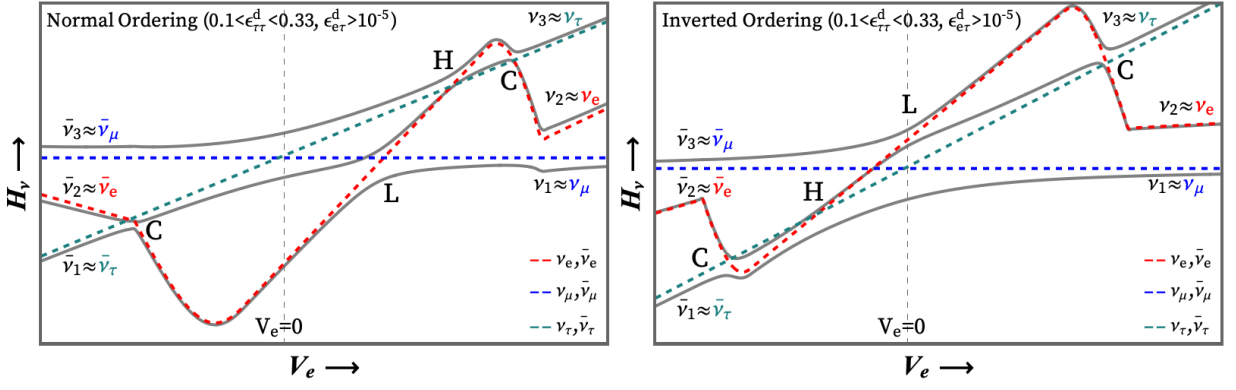


FIG. 4. Configuration of energy levels for neutrinos and antineutrinos for NO (left) and IO (right) with the inclusion of $0.1 < \epsilon_{\tau\tau}^d < 0.33$ and $\epsilon_{e\tau}^d > 10^{-5}$. The MSW resonance locations are marked by the letters *L* and *H*, while the NSI-triggered resonance location is marked by the letter *C*.

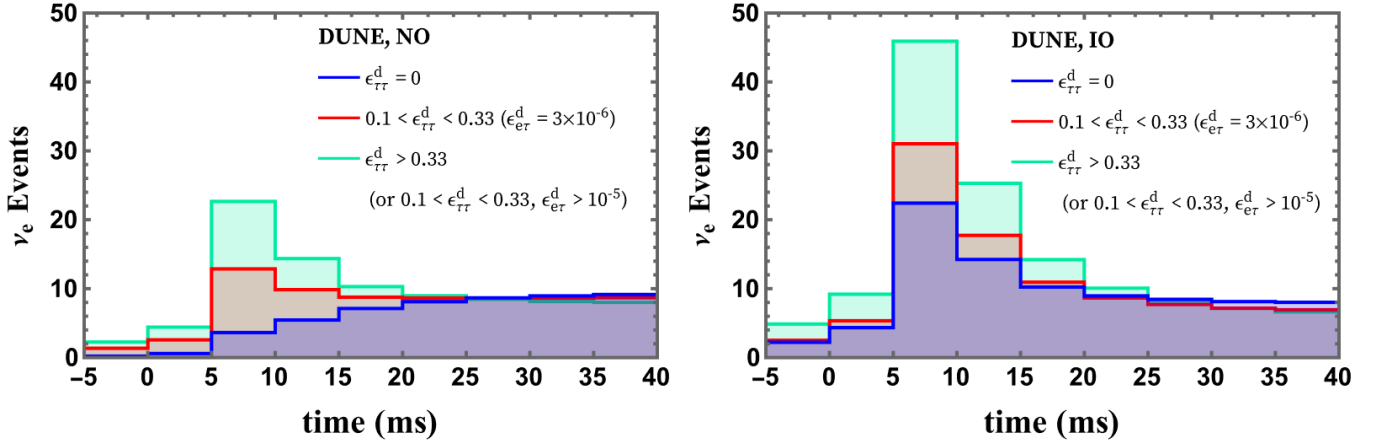


FIG. 5. Expected number of ν_e events per bin of 5 ms at DUNE in the time interval from -5 to 40 ms corresponding to the neutronization burst phase for NO (left) and IO (right). 0 ms represents the time of core bounce. Blue lines are computed from fluxes in Eqs. 7 and 8, assuming the distance between the SN and Earth to be 10 Kpc. Green lines are computed from fluxes modified by the presence of $\epsilon_{\tau\tau}^d > 0.33$ in Eqs. 13 and 14. The similarity between the green line on the left panel and the blue line on the right panel displays the degeneracy between the NO+NSI and standard IO cases. Red lines are computed from fluxes modified by the presence of $0.1 < \epsilon_{\tau\tau}^d < 0.33$ and $10^{-6} < \epsilon_{e\tau} < 10^{-5}$. For $\epsilon_{e\tau}$ in such interval, counting rates are intermediate between the NSI case with $\epsilon_{\tau\tau} > 0.33$ and the standard scenario. For the totally adiabatic *C*-resonance ($\epsilon_{e\tau} > 10^{-5}$), results are degenerate with the ones for $\epsilon_{\tau\tau} > 0.33$.

of total adiabaticity, the produced ν_e reaches vacuum as $\nu_2(\nu_1)$ for NO (IO). The scenario is analogous to the one stated in the last section by Eq. 13 and Eq. 14. When adiabaticity is totally violated, the results are identical to the standard case in Eq. 7 and Eq. 8. Partial adiabaticity provides fluxes, which are intermediary between the standard scenario and the $\epsilon_{\tau\tau}^d > 0.33$ scenario. In the next section, we analyze these signals in DUNE.

We want to stress here that the search for $\epsilon_{\tau\tau}^{u,d}$ during the neutronization burst phase is limited to values of $\mathcal{O}(0.1)$. Conversely, in later phases of SN neutrino emission, when Y_e can attain values below $\mathcal{O}(0.1)$, smaller values of $\epsilon_{\tau\tau}^{u,d}$ could potentially alter observables. Note

that for $Y_e \ll 1$, Eq. 10 and Eq. 11 transforms as:

$$\epsilon_{\tau\tau}^{eff} \approx 2 \frac{\epsilon_{\tau\tau}^d}{Y_e} \quad \text{and} \quad \epsilon_{\tau\tau}^{eff} \approx \frac{\epsilon_{\tau\tau}^u}{Y_e}. \quad (19)$$

Consequently, $\epsilon_{\tau\tau}^{u,d}$ can be as small as $Y_e \sim \mathcal{O}(0.01)$, while maintaining the $\epsilon_{\tau\tau}^{eff}$ value of order one necessary to satisfy the resonance criterion in Eq. 17. Therefore, sensitivity to $\epsilon_{\tau\tau}^{u,d}$ can be improved to $\mathcal{O}(0.01)$ by further investigating flavor conversion that occurs during other phases of neutrino emission.

Signal analysis at DUNE.— Here, we investigate the expected SN neutrino signal spectrum at DUNE under both the standard scenario and the consideration of NSI effects. The graphical representation of the analysis, depicted in Fig. 5, illustrates the projected number of ν_e

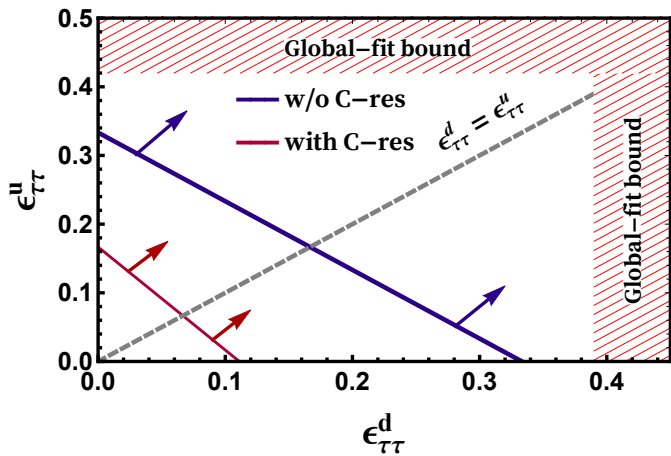


FIG. 6. Projected sensitivities for NSI $\varepsilon_{\tau\tau}$ at DUNE. For the totally adiabatic C -resonance, we consider $\varepsilon_{e\tau} > 10^{-5}$. Global-fit bound on NSI, as shown by the hatched region, is adopted from Ref. [45].

events per 5 ms interval within the time range of -5 to 40 ms (with 0 ms denoting the moment of core bounce). The scenarios for Normal Ordering (NO) and Inverted Ordering (IO) are presented on the left and right sides, respectively, assuming a distance of 10 Kpc between the supernova (SN) and Earth. For detailed information regarding the computation of DUNE event spectra, see the Appendix. The initial neutrino fluxes (F_e^i and F_x^i) are taken from a simulation of a 15 solar mass progenitor [46], as outlined in [17, 19]. The standard case, represented by the blue lines in Fig. 5 [cf. Eq. 7 and Eq. 8], highlights a notable feature—the visibility of the neutronization peak, which distinguishes between the two mass orderings. The green lines are computed from Eq. 13 and Eq. 14 which includes NSI ($\varepsilon_{e\tau}^d > 0.33$). Crucially, as evident from Eq. 8 and Eq. 13, along with Fig. 5, the introduction of NSI leads to a scenario where perfect confusion arises between the two mass orderings (green lines on the left panel and blue lines on the right panel are identical).

DUNE can distinguish between the standard case and signals characterized by $\varepsilon_{\tau\tau}^d > 0.33$, as depicted in each panel of Fig. 5. We analyze it using the χ^2 estimator,

$$\chi^2 = \min_{\xi} \left(\sum_{i=1}^n 2 \left[(1 + \xi)F_i - D_i + D_i \ln \left(\frac{D_i}{(1 + \xi)F_i} \right) \right] \right). \quad (20)$$

F_i and D_i are the number of ν_e events in the i -th time bin for $\varepsilon_{\tau\tau}^d > 0.33$ and $\varepsilon_{\tau\tau}^d = 0$, respectively. The parameter ξ is allowed to vary in the range $-1 < \xi \leq 1000$ with no penalty and we select the minimum to make our derived sensitivity as much as possible independent of the overall normalization. We find for NO,

$$\chi^2(NO) \approx 27, \quad (21)$$

and, for IO,

$$\chi^2(IO) \approx 11. \quad (22)$$

Notably, $\chi^2(NO)$ surpasses $\chi^2(IO)$ by a considerable margin. This discrepancy is primarily attributed to the more pronounced differentiation between the green and blue lines in Fig. 5 for NO, arising from the presence (green) or absence (blue) of the peak around ~ 5 ms. Conversely, for IO, both lines incorporate the peak, and the blue line could mimic the green one even without NSI, contingent on different spectral parameters of the supernova. We want to stress that the green lines in Fig. 5 also represent the case of NSI in the range $0.1 < \varepsilon_{\tau\tau}^d < 0.33$ with adiabatic C -resonance ($\varepsilon_{e\tau}^d > 10^{-5}$). Partial adiabaticity of the C -resonance ($10^{-6} < \varepsilon_{e\tau}^d < 10^{-5}$) provides counting rates between the standard scenario and the $\varepsilon_{\tau\tau}^d > 0.33$ scenario; see red lines in Fig. 5. We exclusively analyze scenarios with d -quark NSI. However, for completeness, Fig. 6 displays projected sensitivities considering the presence of both d -quark and u -quark NSIs.

NSI affecting the flavor evolution of SN neutrinos can also be studied in the electron antineutrino ($\bar{\nu}_e$) channel using other future experiments such as Hyper-Kanmiokande [33] and JUNO [35]. Although these experiments will certainly provide more statistics than DUNE, their observations will lack some specific features of the time signal that are present in the ν_e channel (such as the peak at 5 ms) that can be crucial in diagnosing the presence of NSI. The quark NSI we discussed, which is capable of inducing resonant flavor conversion of supernova neutrinos, may also be subject to complementary tests. For instance, it could produce a Glashow-like resonance feature detectable by neutrino telescopes [47–49] or be examined in future collider experiments, potentially resolving existing degeneracies [50].

Conclusions.— We have shown that the NSIs have a profound impact on supernova neutrino flavor conversion, significantly impacting the neutronization burst signals. The presence of NSI can invert the energy levels of neutrino matter eigenstates and even induce a new resonance in the inner parts close to the proto-neutron star. We showcase how the forthcoming experiments, such as DUNE, can exploit these altered energy level configurations to achieve sensitivity to NSIs at the order of $\mathcal{O}(0.1)$. Furthermore, we elaborate on how this phenomenon may lead to a puzzling ambiguity between normal and inverted mass orderings, and we thoroughly analyze its potential implications.

Acknowledgments.— We are grateful to André de Gouvêa for an illuminating discussion and email correspondence. We also thank Pedro A. N. Machado and Manibrata Sen for useful discussions. We wish to acknowledge the Center for Theoretical Underground Physics and Related Areas (CETUP*) and the Institute for Underground Science at SURF for hospitality and for providing a stimulating environment. The work of YP was supported by the São Paulo Research Foundation (FAPESP) Grant No. 2023/10734-3 and 2023/01467-1 and by the National Council for Scientific and Technological Development (CNPq) Grant No. 151168/2023-7.

S.J. thanks Centro de Ciências Naturais e Humanas at Universidade Federal do ABC and ICTP South American Institute for Fundamental Research for their warm hospitality during the completion of this work.

APPENDICES

1. Neutronization burst phase

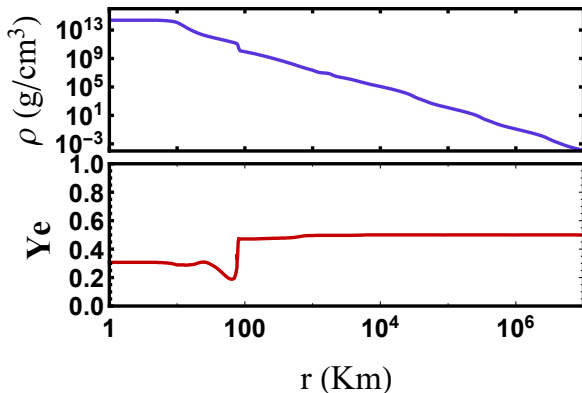


FIG. 7. Status of the matter density ρ and electron number fraction Y_e at 4.37 ms after core bounce. [18, 51].

The SN neutronization burst phase encompasses the period of ~ 40 ms after core bounce when the ν_e luminosity dominates over all other flavors, $\bar{\nu}_e$, ν_x and $\bar{\nu}_x$, with $x = \mu, \tau$ (ν_e luminosity can be 10–100 times higher than luminosity in other flavors, see [17, 19]). During the core collapse, the inner core is compressed and reaches nuclear densities, while the matter falling above it bounces back and launches a shock wave, which dissociates nuclei into its component nucleons as it travels outwards. The capture of electrons in the environment by the dissociated protons, $e^- + p \rightarrow n + \nu_e$, is responsible for generating the large ν_e burst during the neutronization burst phase. Theoretical uncertainties in the calculation of the neutronization fluxes are believed to be as small and 10% [51–54] and uncertainties related to neutrino-neutrino refraction [55, 56] can also be avoided. Therefore, the burst phase presents a great opportunity to search for

new physics with SN neutrinos.

Neutrinos are produced in the region $r < 100$ Km, which is opaque due to very high densities ($\rho > 10^{11}$ g/cm³), and, at $r \sim 100$ Km, they start free streaming. The efficient electron capture at the production region reduces its electron number fraction, $Y_e = n_e/(n_p + n_n)$, where n_e , n_p and n_n are the electron, proton, and neutron number densities, respectively, to levels below the one found in the envelope ($Y_e = 0.5$). Precisely, this difference between Y_e in inner and outer layers might produce observable consequences for non-zero NSI. Further details can be seen in Fig. 7, where we plot ρ and Y_e at ~ 5 ms [18, 57]. This instant is representative of the matter profile during the neutronization peak, the most distinct feature of the burst phase.

2. DUNE: technical details

The Deep Underground Neutrino Experiment (DUNE) will be composed of four-time projection chambers, each with 10 Kton of liquid argon, placed underground in the Long-Baseline Neutrino Facility (LBNF) in South Dakota, United States [36, 37]. DUNE will primarily detect neutrinos with energies of GeV and higher coming from a beam produced at Fermilab. Nevertheless, DUNE is also sensitive to SN neutrinos in the range from about 5 MeV to tens of MeV via the charged-current interaction

$$\nu_e + {}^{40}\text{Ar} \rightarrow {}^{40}\text{K}^* + e^-, \quad (23)$$

that separates the electron flavor and has a much higher cross-section than the elastic scattering, $\nu_{e,\mu,\tau} + e^- \rightarrow \nu_{e,\mu,\tau} + e^-$, which is the current main detection channel for ν_e [38, 58]. We compute the event spectrum for ν_e at DUNE as [59]

$$\frac{dN_{\nu_e}}{dE_r} = \frac{N_{\text{Ar}}}{4\pi R^2} \int dE_{\nu_e} F_{\nu_e}(E_{\nu_e}) \sigma_{\nu_e+\text{Ar}}(E_{\nu_e}) W(E_r, E_{\nu_e}) \quad (24)$$

where N_{Ar} is the number of target ${}^{40}\text{Ar}$ nuclei in the chambers, R is the distance between the SN and the Earth, F_{ν_e} is the ν_e flux leaving the SN with energy E_{ν_e} , $\sigma_{\nu_e+\text{Ar}}$ is the cross section for the interaction in Eq. 23 generated by MARLEY [60], W is the gaussian energy resolution with $\sigma_E/\text{MeV} = 0.11\sqrt{E_r/\text{MeV}} + 0.02E_r/\text{MeV}$ and E_r is the reconstructed electron energy.

-
- [1] L. Wolfenstein, “*Neutrino Oscillations in Matter*,” *Phys. Rev. D* **17** (1978) 2369–2374.
 [2] O. G. Miranda, M. A. Tortola, and J. W. F. Valle, “*Are solar neutrino oscillations robust?*,” *JHEP* **10** (2006) 008, [arXiv:hep-ph/0406280](#).

- [3] M. Maltoni and A. Y. Smirnov, “*Solar neutrinos and neutrino physics*,” *Eur. Phys. J. A* **52** (2016) no. 4, 87, [arXiv:1507.05287](#).
 [4] S. A. Colgate and R. H. White, “*The Hydrodynamic Behavior of Supernovae Explosions*,” *Astrophys. J.* **143** (1966) 626.

- [5] W. D. Arnett, “Gravitational collapse and weak interactions,” *Can. J. Phys.* **44** (1966) 2553–2594.
- [6] H. A. Bethe and J. R. Wilson, “Revival of a stalled supernova shock by neutrino heating,” *Astrophys. J.* **295** (1985) 14–23.
- [7] J. R. Wilson, “Supernovae and Post-Collapse Behavior,” *Numerical Astrophysics* (1985) 422.
- [8] H. T. Janka, “Neutrino Emission from Supernovae,” [arXiv:1702.08713](https://arxiv.org/abs/1702.08713).
- [9] P. S. B. Dev, S. Jana, and Y. Porto, “Flavor Matters, but Matter Flavors: Matter Effects on Flavor Composition of Astrophysical Neutrinos,” [arXiv:2312.17315](https://arxiv.org/abs/2312.17315).
- [10] S. P. Mikheyev and A. Y. Smirnov, “Resonance Amplification of Oscillations in Matter and Spectroscopy of Solar Neutrinos,” *Sov. J. Nucl. Phys.* **42** (1985) 913–917.
- [11] S. P. Mikheev and A. Y. Smirnov, “Resonant amplification of neutrino oscillations in matter and solar neutrino spectroscopy,” *Nuovo Cim. C* **9** (1986) 17–26.
- [12] S. P. Mikheev and A. Y. Smirnov, “Neutrino Oscillations in a Variable Density Medium and Neutrino Bursts Due to the Gravitational Collapse of Stars,” *Sov. Phys. JETP* **64** (1986) 4–7, [arXiv:0706.0454](https://arxiv.org/abs/0706.0454).
- [13] J. W. F. Valle, “Resonant Oscillations of Massless Neutrinos in Matter,” *Phys. Lett. B* **199** (1987) 432–436.
- [14] H. Nunokawa, J. T. Peltoniemi, A. Rossi, and J. W. F. Valle, “Supernova bounds on resonant active sterile neutrino conversions,” *Phys. Rev. D* **56** (1997) 1704–1713, [arXiv:hep-ph/9702372](https://arxiv.org/abs/hep-ph/9702372).
- [15] H. Nunokawa, R. Tomas, and J. W. F. Valle, “Type II supernovae and neutrino magnetic moments,” *Astropart. Phys.* **11** (1999) 317–325, [arXiv:astro-ph/9811181](https://arxiv.org/abs/astro-ph/9811181).
- [16] A. Esteban-Pretel, R. Tomas, and J. W. F. Valle, “Probing non-standard neutrino interactions with supernova neutrinos,” *Phys. Rev. D* **76** (2007) 053001, [arXiv:0704.0032](https://arxiv.org/abs/0704.0032).
- [17] A. de Gouvêa, I. Martinez-Soler, and M. Sen, “Impact of neutrino decays on the supernova neutronization-burst flux,” *Phys. Rev. D* **101** (2020) no. 4, 043013, [arXiv:1910.01127](https://arxiv.org/abs/1910.01127).
- [18] J. Tang, T. Wang, and M.-R. Wu, “Constraining sterile neutrinos by core-collapse supernovae with multiple detectors,” *JCAP* **10** (2020) 038, [arXiv:2005.09168](https://arxiv.org/abs/2005.09168).
- [19] S. Jana, Y. P. Porto-Silva, and M. Sen, “Exploiting a future galactic supernova to probe neutrino magnetic moments,” *JCAP* **09** (2022) 079, [arXiv:2203.01950](https://arxiv.org/abs/2203.01950).
- [20] S. Jana and Y. Porto, “Resonances of Supernova Neutrinos in Twisting Magnetic Fields,” *Phys. Rev. Lett.* **132** (2024) no. 10, 101005, [arXiv:2303.13572](https://arxiv.org/abs/2303.13572).
- [21] M. V. dos Santos, P. C. de Holanda, P. Dedin Neto, and E. Kemp, “Effects of quantum decoherence in a future supernova neutrino detection,” *Phys. Rev. D* **108** (2023) no. 10, 103032, [arXiv:2306.17591](https://arxiv.org/abs/2306.17591).
- [22] M. Bendahman *et al.*, “Prospects for realtime characterization of core-collapse supernova and neutrino properties,” [arXiv:2311.06216](https://arxiv.org/abs/2311.06216).
- [23] G. A. Tammann, W. Loeffler, and A. Schroder, “The Galactic supernova rate,” *Astrophys. J. Suppl.* **92** (1994) 487–493.
- [24] **Kamiokande-II**, K. Hirata *et al.*, “Observation of a Neutrino Burst from the Supernova SN 1987a,” *Phys. Rev. Lett.* **58** (1987) 1490–1493.
- [25] R. M. Bionta *et al.*, “Observation of a Neutrino Burst in Coincidence with Supernova SN 1987a in the Large Magellanic Cloud,” *Phys. Rev. Lett.* **58** (1987) 1494.
- [26] E. N. Alekseev, L. N. Alekseeva, I. V. Krivosheina, and V. I. Volchenko, “Detection of the Neutrino Signal From SN1987A in the LMC Using the Inr Baksan Underground Scintillation Telescope,” *Phys. Lett. B* **205** (1988) 209–214.
- [27] J. Olsen and Y.-Z. Qian, “Comparison of simulated neutrino emission models with data on Supernova 1987A,” *Phys. Rev. D* **104** (2021) no. 12, 123020, [arXiv:2108.08463](https://arxiv.org/abs/2108.08463). [Erratum: *Phys.Rev.D* 106, 109904 (2022)].
- [28] S. W. Li, J. F. Beacom, L. F. Roberts, and F. Capozzi, “Old Data, New Forensics: The First Second of SN 1987A Neutrino Emission,” [arXiv:2306.08024](https://arxiv.org/abs/2306.08024).
- [29] P. Dedin Neto, M. V. d. Santos, P. C. de Holanda, and E. Kemp, “SN1987A neutrino burst: limits on flavor conversion,” *Eur. Phys. J. C* **83** (2023) no. 6, 459, [arXiv:2301.11407](https://arxiv.org/abs/2301.11407).
- [30] D. F. G. Fiorillo, M. Heinlein, H.-T. Janka, G. Raffelt, E. Vitagliano, and R. Bollig, “Supernova simulations confront SN 1987A neutrinos,” *Phys. Rev. D* **108** (2023) no. 8, 083040, [arXiv:2308.01403](https://arxiv.org/abs/2308.01403).
- [31] **IceCube**, R. Abbasi *et al.*, “IceCube Sensitivity for Low-Energy Neutrinos from Nearby Supernovae,” *Astron. Astrophys.* **535** (2011) A109, [arXiv:1108.0171](https://arxiv.org/abs/1108.0171). [Erratum: *Astron.Astrophys.* 563, C1 (2014)].
- [32] **DarkSide 20k**, P. Agnes *et al.*, “Sensitivity of future liquid argon dark matter search experiments to core-collapse supernova neutrinos,” *JCAP* **03** (2021) 043, [arXiv:2011.07819](https://arxiv.org/abs/2011.07819).
- [33] **Hyper-Kamiokande**, K. Abe *et al.*, “Supernova Model Discrimination with Hyper-Kamiokande,” *Astrophys. J.* **916** (2021) no. 1, 15, [arXiv:2101.05269](https://arxiv.org/abs/2101.05269).
- [34] **KM3NeT**, S. Aiello *et al.*, “The KM3NeT potential for the next core-collapse supernova observation with neutrinos,” *Eur. Phys. J. C* **81** (2021) no. 5, 445, [arXiv:2102.05977](https://arxiv.org/abs/2102.05977).
- [35] **JUNO**, A. Abusleme *et al.*, “Real-time Monitoring for the Next Core-Collapse Supernova in JUNO,” [arXiv:2309.07109](https://arxiv.org/abs/2309.07109).
- [36] **DUNE**, B. Abi *et al.*, “Supernova neutrino burst detection with the Deep Underground Neutrino Experiment,” *Eur. Phys. J. C* **81** (2021) no. 5, 423, [arXiv:2008.06647](https://arxiv.org/abs/2008.06647).
- [37] **DUNE**, C. Cuesta, “Supernova and solar neutrino searches at DUNE,” in *18th International Conference on Topics in Astroparticle and Underground Physics*. 11, 2023. [arXiv:2311.06134](https://arxiv.org/abs/2311.06134).
- [38] G. Zhu, S. W. Li, and J. F. Beacom, “Developing the MeV potential of DUNE: Detailed considerations of muon-induced spallation and other backgrounds,” *Phys. Rev. C* **99** (2019) no. 5, 055810, [arXiv:1811.07912](https://arxiv.org/abs/1811.07912).
- [39] S. P. Mikheev and A. Y. Smirnov, “Neutrino Oscillations in an Inhomogeneous Medium: Adiabatic Regime,” *Sov. Phys. JETP* **65** (1987) 230–236.
- [40] I. Esteban, M. C. Gonzalez-Garcia, M. Maltoni, I. Martinez-Soler, and J. Salvado, “Updated constraints on non-standard interactions from global analysis of oscillation data,” *JHEP* **08** (2018) 180,

- arXiv:1805.04530. [Addendum: JHEP 12, 152 (2020)].
- [41] A. S. Dighe and A. Y. Smirnov, “Identifying the neutrino mass spectrum from the neutrino burst from a supernova,” *Phys. Rev. D* **62** (2000) 033007, arXiv:hep-ph/9907423.
- [42] K. S. Babu, P. S. B. Dev, S. Jana, and A. Thapa, “Non-Standard Interactions in Radiative Neutrino Mass Models,” *JHEP* **03** (2020) 006, arXiv:1907.09498.
- [43] S. S. Chatterjee and A. Palazzo, “Nonstandard Neutrino Interactions as a Solution to the $NO\nu A$ and $T2K$ Discrepancy,” *Phys. Rev. Lett.* **126** (2021) no. 5, 051802, arXiv:2008.04161.
- [44] P. B. Denton, J. Gehrlein, and R. Pestes, “ CP -Violating Neutrino Nonstandard Interactions in Long-Baseline-Accelerator Data,” *Phys. Rev. Lett.* **126** (2021) no. 5, 051801, arXiv:2008.01110.
- [45] P. Coloma, M. C. Gonzalez-Garcia, M. Maltoni, J. a. P. Pinheiro, and S. Urrea, “Global constraints on non-standard neutrino interactions with quarks and electrons,” *JHEP* **08** (2023) 032, arXiv:2305.07698.
- [46] “Garching Core-Collapse Supernova Archive,”
<https://wwwmpa.mpa-garching.mpg.de/ccsnarchive/>.
- [47] K. S. Babu, P. S. B. Dev, and S. Jana, “Probing neutrino mass models through resonances at neutrino telescopes,” *Int. J. Mod. Phys. A* **37** (2022) no. 11n12, 2230003, arXiv:2202.06975.
- [48] K. S. Babu, P. S. Dev, S. Jana, and Y. Sui, “Zee-Burst: A New Probe of Neutrino Nonstandard Interactions at IceCube,” *Phys. Rev. Lett.* **124** (2020) no. 4, 041805, arXiv:1908.02779.
- [49] G.-y. Huang, S. Jana, M. Lindner, and W. Rodejohann, “Probing new physics at future tau neutrino telescopes,” *JCAP* **02** (2022) no. 02, 038, arXiv:2112.09476.
- [50] K. S. Babu, D. Gonçalves, S. Jana, and P. A. N. Machado, “Neutrino Non-Standard Interactions: Complementarity Between LHC and Oscillation Experiments,” *Phys. Lett. B* **815** (2021) 136131, arXiv:2003.03383.
- [51] P. D. Serpico, S. Chakraborty, T. Fischer, L. Hudepohl, H.-T. Janka, and A. Mirizzi, “Probing the neutrino mass hierarchy with the rise time of a supernova burst,” *Phys. Rev. D* **85** (2012) 085031, arXiv:1111.4483.
- [52] J. Wallace, A. Burrows, and J. C. Dolence, “Detecting the Supernova Breakout Burst in Terrestrial Neutrino Detectors,” *Astrophys. J.* **817** (2016) no. 2, 182, arXiv:1510.01338.
- [53] E. O’Connor *et al.*, “Global Comparison of Core-Collapse Supernova Simulations in Spherical Symmetry,” *J. Phys. G* **45** (2018) no. 10, 104001, arXiv:1806.04175.
- [54] M. Kachelriess, R. Tomas, R. Buras, H. T. Janka, A. Marek, and M. Rampp, “Exploiting the neutronization burst of a galactic supernova,” *Phys. Rev. D* **71** (2005) 063003, arXiv:astro-ph/0412082.
- [55] A. Mirizzi, I. Tamborra, H.-T. Janka, N. Saviano, K. Scholberg, R. Bollig, L. Hudepohl, and S. Chakraborty, “Supernova Neutrinos: Production, Oscillations and Detection,” *Riv. Nuovo Cim.* **39** (2016) no. 1-2, 1–112, arXiv:1508.00785.
- [56] A. Capanema, Y. Porto, and M. M. Saez, “The Flavor Composition of Supernova Neutrinos,” arXiv:2403.14762.
- [57] T. Fischer, S. C. Whitehouse, A. Mezzacappa, F. K. Thielemann, and M. Liebendorfer, “Protoneutron star evolution and the neutrino driven wind in general relativistic neutrino radiation hydrodynamics simulations,” *Astron. Astrophys.* **517** (2010) A80, arXiv:0908.1871.
- [58] K. Scholberg, “Supernova Neutrino Detection,” *Ann. Rev. Nucl. Part. Sci.* **62** (2012) 81–103, arXiv:1205.6003.
- [59] F. Capozzi, B. Dasgupta, and A. Mirizzi, “Model-independent diagnostic of self-induced spectral equalization versus ordinary matter effects in supernova neutrinos,” *Phys. Rev. D* **98** (2018) no. 6, 063013, arXiv:1807.00840.
- [60] S. J. Gardiner, *Nuclear Effects in Neutrino Detection*. PhD thesis, UC, Davis, 2018.